Available online at www.sciencedirect.com

SCIENCE DIRECT

Biochimica et Biophysica Acta 1668 (2005) 106–116

BIOCHIMICA ET BIOPHYSICA ACTA BBA

http://www.elsevier.com/locate/bba

# A model of sodium channels

Taira Vora[a], Ben Corry[b], Shin-Ho Chung[a,*]

[a]Department of Theoretical Physics, Research School of Physical Sciences, Australian National University, Canberra, A.C.T. 0200, Australia
[b]Department of Chemistry, University of Western Australia, Crawley, WA, 6009, Australia

Received 16 December 2003; received in revised form 6 July 2004; accepted 16 November 2004
Available online 2 December 2004

**Abstract**

We have explored the permeation and blockage of ions in sodium channels, relating the channel structure to function using electrostatic profiles and Brownian dynamics simulations. The model used resembles the KcsA potassium channel with an added external vestibule and a shorter selectivity filter. The electrostatic energy landscape seen by permeating ions is determined by solving Poisson's equation. The two charged amino acid rings of Glu-Glu-Asp-Asp (EEDD) and Asp-Glu-Lys-Ala (DEKA) around the selectivity filter region are seen to play a crucial role in making the channel sodium selective, and strongly binding calcium ions such that they block the channel. Our model closely reproduces a range of experimental data including the current–voltage curves, current–concentration curves and blockage of monovalent ions by divalent ions.


*Keywords:* Sodium channel; Permeation; Ion channel; Brownian dynamics; Electrostatics; Blockage; Selectivity

## 1. Introduction

Sodium channels are widely dispersed across the body, from neurons in the brain and body, to vertebrate skeletal and cardiac muscles, and endocrine glands. Although responsible for a vast array of important bodily functions their primary role is the conduction of action potentials. There is a huge variety of sodium conductive channels, but here we deal with the voltage-gated channels to which this term is usually applied. Most sodium channels conserve the EEDD and DEKA ring of residues believed to line the selectivity filter region. Another common feature of the sodium channel family is its very small conductance of between 10 and 30 pS. This range is seen in the sodium channels in cardiac tissue, myelinated nerve fibres, giant squid axon and brain planar lipid bilayers [1–16,18]. In this paper, we aim to construct a model of the family of voltage-gated sodium channels that can relate its physical and functional properties. Since no crystal structure exists for the family of sodium channels, we base our model on information gathered from the crystal structure of similar channels as well as patch clamp and theoretical models, and examine what structures can reproduce the properties of this channel. Mutation studies reveal that the most important structural feature is the two rings of charged amino acids around the narrow selectivity filter, responsible for the channel's affinity for sodium ions [19–22] and, as we discuss later, block by divalent ions. We have constructed a model using information gathered from molecular models [22–24], cryo-electron microscopy [26] and the recently crystallized KcsA channel [27]. By performing Brownian dynamics (BD) simulations, we are able to reproduce the experimental current–voltage, current–concentration and blockage results, and highlight the important structural features responsible for the various functions of the channel.

## 2. Methods

### 2.1. Channel model

The first, and possibly the most important, part of the simulation process is creating a shape of the channel that

* Corresponding author. Tel.: +61 2 6249 2024; fax: +61 2 6247 2792.
*E-mail address:* shin-ho.chung@anu.edu.au (S.-H. Chung).

0005-2736/$ - see front matter © 2004 Elsevier B.V. All rights reserved.
doi:10.1016/j.bbamem.2004.11.011

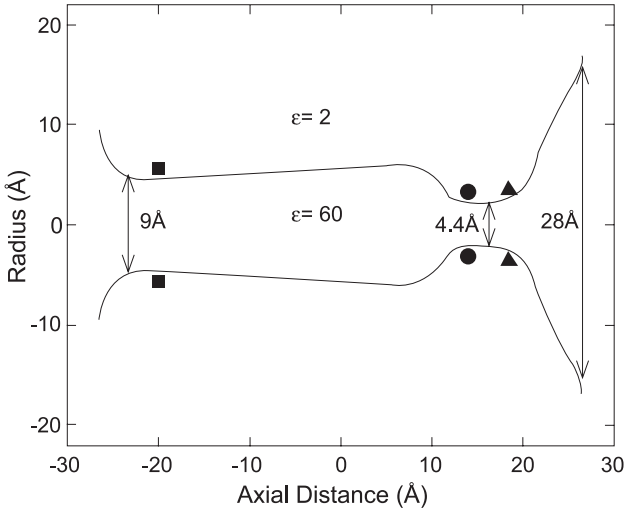


Fig. 1. Sodium channel model. The sodium channel model is generated by rotating each curve by 180°. The points marked by the triangles and circles around the selectivity filter represent the position of the two rings of EEDD and DEKA residues, respectively. The squares correspond to the negative dipoles at the end of the protein.

resembles its structure. We base our model on the gross structure of the KcsA channel [27]. However, as seen in Fig. 1A, we shorten the length of the selectivity filter to be only about 4 Å and add a funnel-shaped extracellular vestibule formed by the P loops near the extracellular side of the protein with a radius of $r$=14 Å. The shape and dimensions were adopted from molecular models presented by Guy and Durell [24] and Lipkind and Fozzard [25]. The narrowest region of our model is the selectivity filter, the radius of which is set to $r$=2.2 Å. This value is chosen to correspond to the minimum cross-sectional area suggested by examining the permeability of various organic cations [28]. The total length of the channel is 53 Å with a large intracellular entrance (similar to that of KcsA) of diameter 9 Å near the intracellular mouth.

Changing any of these parameters has an acute affect on the conductance properties of the channel. For example, enlarging the diameter of the inner pore to 10 Å dramatically increases the outward current, as intracellular sodium ions find it easier to enter the channel due to smaller repulsive image forces from the dielectric boundary. Also, when the diameter of the central chamber, currently set at 12 Å, is increased, the current becomes highly asymmetric with the outward current much higher than the inward current. Thus, once the gross features of the channel are specified, only a small range of possible dimensions can reproduce experimental data.

As we do not have the detailed atomic structure of the protein, rather than including all the partial charges of the protein atoms, we include only a selection of important charges as has been done successfully in previous models of potassium and calcium channels [29,30]. There are two important rings of charged amino acid residues believed to line the selectivity filter as mutations of these significantly affect the conductance and selectivity of the channel [19–22]. We model these as point charges placed 1 Å behind the channel boundary. The outer ring of EEDD residues lies at $z$=18.5 Å and the inner ring of DEKA residues lies at $z$=14 Å. Determining the charge state of these residues is not straightforward in the complex channel environment. We expect the positive lysine residue in the inner ring to be fully charged, but one or more of the other negatively charged residues may become protonated. To determine the most likely charge state of the channel, we calculate the current passing through the channel with various combinations of charges on these rings. To do this, we hold the charge on one ring constant while varying the charge on the other. An example of this is shown in Fig. 2. In Fig. 2A we hold the charge on the outer ring fixed at $-3.8\times10^{-19}$ C and

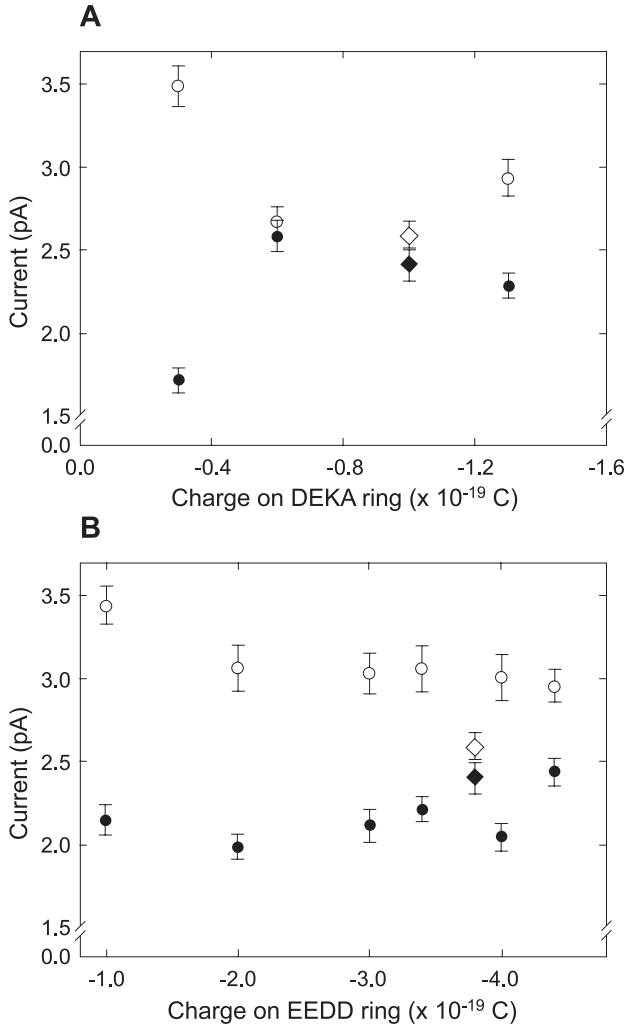


Fig. 2. Influence of partial charges on channel conductance. The magnitude of current passing through the channel for each charge combination obtained from simulations at +106 mV (filled symbols) and −94 mV (open symbols). (A) The total charge of the inner ring of DEKA residues is varied between $-0.3\times10^{-19}$ and $-1.3\times10^{-19}$ C while the outer ring of EEDD residues is kept fixed at $-3.8\times10^{-19}$ C. (B) The total charge of the outer ring of EEDD residues is varied between $-1.0\times10^{-19}$ and $-4.4\times10^{-19}$ C while inner ring is fixed at $-1.0\times10^{-19}$ C.

systematically vary the charge on the inner ring. The total current passing through the channel at +106 and −94 mV is shown by the filled and open symbols, respectively. Similarly, in Fig. 2B we hold the charge on the inner ring fixed at $-1\times10^{-19}$ C and calculate the current passing through the channel while varying the charge on the outer ring.

Using this method, we find that the best agreement with experimental data (i.e., symmetric currents of the correct magnitude) is obtained when on average two of the residues are protonated. In particular, the best results are obtained when the outer ring has a total charge of $-3.8\times10^{-19}$ C and the inner ring a charge of $-1\times10^{-19}$ C, indicated by filled and open diamonds in Fig. 2. These charges are spread evenly across the residues in each ring so that the four negatively charged residues in the outer ring each have charges of $-0.95\times10^{-19}$ C, while the aspartate and glutamate residues of the inner ring both have a charge of $-1.3\times10^{-19}$ C. A number of combinations of charge per ring were tried in addition to those shown in Fig. 2 but they only enforced the fact that the combination stated above is unique. While a few other combinations do succeed in reproducing the experimental conductance, we found that of the combinations we tried, only this one could qualitatively reproduce the block of sodium current by calcium ions described later.

Four dipole charges of $0.6\times10^{-19}$ C each are also introduced at the intracellular pore end of the channel with their negative ends facing the channel to represent the macroscopic helix dipoles. These dipoles aid the entry of ions into the narrow intracellular end of the channel. Therefore, we conclude that only a very small range of charge positions and magnitudes can reproduce the experimental data of conductance, current–concentration and blocking by divalent ions.

### 2.2. Simulation details

Once a model channel has been created, we perform BD simulations to obtain the channel conductance. In these simulations, we place a number of Na and Cl ions in reservoirs attached to either end of the channel to represent the intracellular and extracellular space. We then simulate the motion of the ions under the influence of electric, random and frictional forces using the Langevin equation,

$$m_i \frac{d\mathbf{v}_i}{dt} = -m_i\gamma_i\mathbf{v}_i + \mathbf{F}_R(t) + q_i\mathbf{E}_i + \mathbf{F}_S \quad (1)$$

The first term on the right describes the frictional force experienced by an ion as it attempts to move through a fluid with a frictional coefficient of $m_i\gamma_i$. The second term, $\mathbf{F}_R(t)$, is a random force arising from collisions of the ions with water molecules that are not treated explicitly in our simulations. The last term $\mathbf{F}_S$ is a short-range force term that includes short range ion–ion and ion–wall interactions [29].

The electrical force acting on an ion, $q_i\mathbf{E}_i$, includes the potential applied across the channel as well as the Coulomb interaction between the ions and the fixed charges in the protein, and the image charges induced along the water–protein boundaries. These electrical forces can be calculated by solving Poisson's equation:

$$\varepsilon_0\nabla[\varepsilon(\mathbf{r})\nabla\phi(\mathbf{r})] = -\rho(\mathbf{r}) \quad (2)$$

in which $\varepsilon(\mathbf{r})$, $\phi(\mathbf{r})$, and $\rho(\mathbf{r})$ are the space-dependent dielectric constant, electric potential and charge density. This equation can be solved analytically for only a handful of channel shapes, and for the model used here a numerical iterative 'boundary element' technique is used [32,33]. To do this computation a dielectric constant of $\varepsilon$=2 is assigned to the channel protein and $\varepsilon$=60 to the water in the channel and reservoirs [31,37]. Although a value of 80 should be assigned to the bulk solution in the reservoirs, this causes problems for the numerical solutions as ions cross the dielectric boundary to enter the channel. Thus, an artificial Born energy barrier is introduced at the entrance and exit of the channel to compensate for this [31,37].

We implemented the Langevin equation using an algorithm devised by van Gunsteren et al. [35,36]. A time step of 100 fs is used to trace the path of ions through the channel and a larger time step of 2 ps for ions in the reservoirs. To save calculating the forces on every ion at every step during the simulation, many of the force components are pre-calculated for various ion configurations and stored in lookup tables [31]. Once the forces are calculated for a given configuration, new positions are calculated for each ion to give their location 2 ps later, and this entire procedure is repeated. The current is determined by counting the number of ions traversing the channel in a given period.

To obtain concentrations of 200 mM used in much of this study, 14 pairs of Na and Cl ions are placed in each reservoir. The number of ions was increased or decreased in order to simulate higher or lower concentrations keeping the size of the reservoirs fixed for all simulations. The values of the physical parameters used in the simulations are given in Table 1. Diffusion coefficients of 0.1 and 0.3 times the bulk value for sodium were used in the outer vestibule and the narrower section (27>$z$>10 Å) and the intracellular chamber (10>$z$>−25 Å) of the channel, respectively, as suggested by molecular dynamics studies of narrow channels [34]. Corresponding values of 0.15 and 0.4 were used for calcium.

In all the simulations involving mixtures of NaCl and $CaCl_2$ in the reservoirs, concentrations of 200 mM and 110

Table 1

| | $Na^+$ | $Ca^{2+}$ | $Cl^-$ |
|---|---|---|---|
| Mass (kg) | $3.8\times10^{-26}$ | $6.6\times10^{-26}$ | $5.9\times10^{-26}$ |
| Bulk diffusion ($m^2$ $s^{-1}$) | $1.33\times10^{-9}$ | $0.79\times10^{-9}$ | $2.03\times10^{-9}$ |
| Ionic radii (Å) | 0.95 | 0.99 | 1.81 |

mM were used, with nine and five pairs of each species. The simulation results have been compared to experimental results obtained by French et al. [16], but we only hope to make a qualitative comparison. Performing simulations with lower concentrations of calcium, such as experimental concentrations of 10 mM, is difficult as it involves taking very few pairs of ions and very large reservoir sizes. This increases the simulation time, as very many $Na^+$ and $Cl^-$ must also be present, and makes it harder to gain statistically reliable results as interactions between the calcium ions and the channel become rarer. The intention of these results is to discuss the general agreement between the experimental and simulated IV curves, as well as to use the model to try and understand the underlying mechanisms responsible for the attenuation of sodium current in the presence of calcium, rather than to make a direct quantitative comparison.

## 3. Results

### 3.1. Sodium permeation

The electrostatic energy profiles for various ion configurations found by solving Poisson's equation with an applied potential of −94 mV are shown in Fig. 3. As a single sodium ion is brought in to the channel from the extracellular side along the channel axis in 1-Å intervals, it sees a deep energy well of 20 kT (solid line) with an energy minimum in the selectivity filter where it is surrounded by the two rings of negatively charged amino acid residues. To pass through the channel, however, the ion must climb out of this well and over an energy barrier 13 kT in height created by the charges it induces in the central hydrophobic section of the channel. This energy barrier is virtually insurmountable by one sodium ion alone in its random thermal motions.

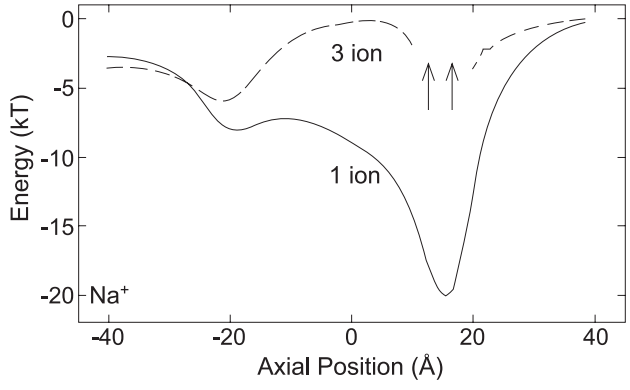


Fig. 3. Potential energy profiles. Potential energy profiles of a single sodium ion (solid line) or with three ions in the channel (dashed lines) are calculated at an applied potential of −94 mV. In the multi-ion profile, an ion is brought into the channel from the right while two ions are allowed to find their minimum energy positions in the selectivity filter (dashed line, right hand side). Once all ions are in the filter, the energy of the left hand ion is calculated as it is moved out to the intracellular side of the channel (dashed line, left hand side).

The channel can, in fact, hold two Na ions in stable equilibrium in the selectivity filter. However, this can be disrupted when a third ion enters. The energy profile seen by a third ion entering the channel from the extracellular side in this situation is indicated by the right hand side of the dashed line in Fig. 3. The third ion still sees an energy well of nearly 3 kT at the mouth of the channel attracting it inside. However, if we now move the left hand ion through to the intracellular end of the channel with the other two ions in the selectivity filter, we find that the central barrier is lowered to only 3.5 kT, which it can be expected to cross in its random motions with the aid of the repulsive forces it experiences from the nearby sodium ions. Therefore, from the electrostatic profiles, it appears that conduction through the channel is likely to be a three-ion process.

Next we determine the conductance properties of the channel using BD simulations. As the current passing through the channel is very small, a large number of simulations are required to obtain reliable results. Thus, each data point represents 13 μs of simulation time. The current–voltage curve shown in Fig. 4A is symmetric and linear through the origin in agreement with most experimental results [1,2,4,7,10,14,15]. The results of Schild et al. [1] are shown in the inset for comparison with our BD data. The simulated data have an outward current at +106 mV of 2.4±0.2 pA, and an inward current at −94 mV of −2.5 pA. The slope conductance of about 24.5 pS agrees well with the experimental value of 21 pS.

Experimental results show that the sodium current through the channel is concentration-dependent but arrives quickly at a saturation value of about 2 pA under a −70 mV driving potential (here again results are taken from Schild and Moczydlowski [2] for comparison) [2,16,17]. This phenomenon is also observed in our simulations. As we vary the concentration in the reservoirs from 75 to 500 mM by adding or removing ions (thus keeping the reservoir the same size for all simulations), the current rapidly saturates. The simulated data are compared to experimental results in Fig. 4B. The agreement between the results is reasonable although some differences in the current can be seen at low concentrations. The simulated data are fitted with a Michaelis–Menton curve [31]:

$$I = \frac{I_{\max}}{1 + K_S/[\mathrm{Na}]} \tag{3}$$

in which [Na] is the sodium ion concentration, $I_{\max}$ is the saturation current and $K_S$ is the half-maximum concentration. The experimental data show a point of half-maximum of $K_S \approx 40$ mM while the simulated value is $K_S$=75 mM [2,16,17]. Thus, although a general agreement is seen between the simulations and experiment, saturation occurs at slightly higher concentrations in the simulated data.

The average distribution of ions in the channel at an applied potential of −70 mV found during BD simulations

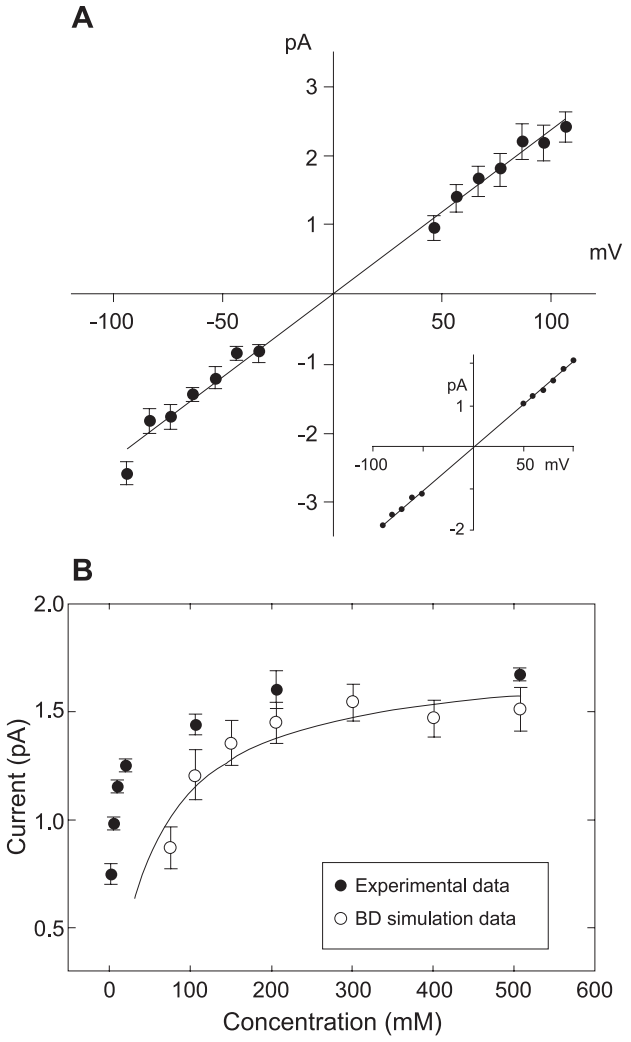


Fig. 4. Current–voltage and current–concentration relationships. (A) The current–voltage curve was obtained with a symmetric solution of 200 mM NaCl. Each data point represents a 13-μs simulation. The inset shows the experimental results obtained under similar conditions by Schild and Moczydlowski [2]. (B) The current–concentration curve obtained from BD simulations (open circles) is plotted against the experimental data (filled circles) obtained by Schild et al. [1] at a driving potential of −70 mV. A Michaelis–Menton curve has been fitted to the simulated data.

is shown in Fig. 5B. The channel has been divided into 100 layers and the average number of ions in each layer during the simulation is indicated. There are approximately 2.5 ions in the channel in total, 1.2 ions situated near the outer ring of charges (EEDD ring), 1 ion at the inner ring of charges (DEKA ring) and approximately 0.3 ions near the intracellular helix dipoles. This also suggests that permeation involves three ions. An ion is also usually found in the external vestibule.

The saturation of current at high concentrations can be easily explained by examining the steps required for permeation. Let $t_1$ (shown in Fig. 5A) be the time taken by an ion to enter the channel while two ions are already occupying the selectivity filter (as this is the equilibrium state). Clearly, this process is accelerated by increasing the number of ions in the reservoirs, that is, at higher concentrations, thereby making this step concentration-dependent. However, $t_2$, the time taken by the first ion in the channel to leave the selectivity filter and move across the central part of the channel once the third ion has entered, does not depend on reservoir concentrations. Rather, this time depends on the kinetic energy of the ion and also the repulsive force provided to it by the other ions in the selectivity filter as they exert random motions. Thus, at high concentrations, although $t_1$ will become very small, $t_2$ will stay the same and limit the conductance of the channel. That crossing the center of the channel is the rate-limiting step is also suggested in Fig. 5B. There are three distinct peaks for the three positions of ions (circles) shown in Fig. 5A illustrating that there is usually an ion present at the external end of the channel as required for conduction. However, there are almost no ions present in the central region of the channel.

### 3.2. Blockage by calcium ions

Experimental results reveal that calcium, in an extracellular solution, interferes with the normal conduction of sodium ions in the open channel [16,17,38–46]. It is believed that the presence of calcium obstructs the sodium ions and prevents conduction. Also, with calcium as the only cation in the solution, the conductance of the sodium channel is greatly reduced, so much so that the ratio of the calcium current to the pure sodium current ($I_{Ca}/I_{Na}$)<0.01 [21].

We performed BD simulations with calcium and sodium ions in solution under three different conditions. These results are presented in Fig. 6 (filled circles), alongside the *I–V* curve for symmetrical concentrations of 200 mM sodium chloride solutions (open circles). For comparison, the figures also contain an inset of the data collected by French et al. [16] under similar conditions. The first set of simulations, shown in Fig. 6A, was carried out with an extracellular mixture of 200 mM sodium chloride and 110 mM calcium chloride and an intracellular solution of only 200 mM sodium chloride. We see a large attenuation in the current into the cell. We notice that the current falls to 0.3±0.1 pA at −94 mV and is reduced to 1.7±0.2 pA at +106 mV. Fig. 6B represents *I–V* results with intracellular sodium and calcium chloride concentrations of 200 mM and 110 mM, respectively, and an extracellular solution of pure 200 mM sodium chloride. This time we see a larger attenuation of the outgoing current from the cell to 1.7±0.2 pA at +106 mV and a reduction in the incoming current to 1.8±0.3 pA. The final set of results shown in Fig. 6C is current measurements at symmetrical concentration of 200 mM sodium chloride and 110 mM calcium chloride. The intracellular current falls to 0.3±0.2 at −94 mV and the extracellular current reduces to 1.4±0.2 pA as shown in Fig. 6C. All of these results are in good agreement with data presented by French et al. [16].

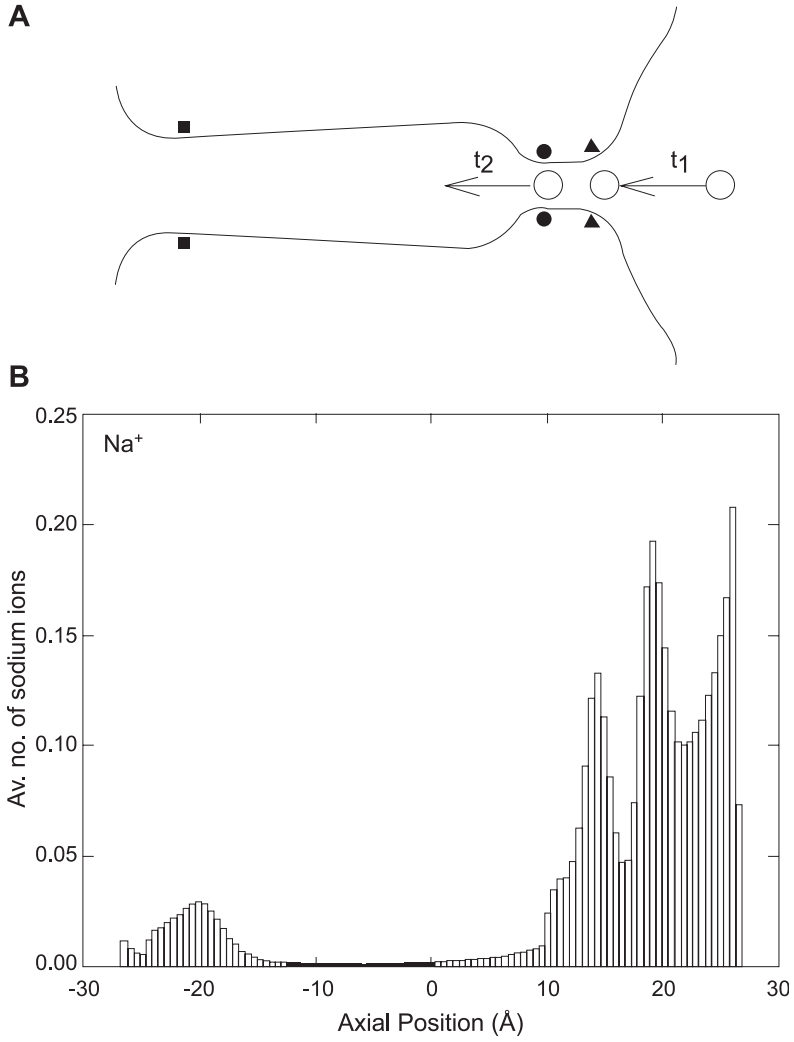


Fig. 5. Average number of sodium ions in the channel at an applied potential of −70 mV (B). There are three distinct peaks corresponding to the positions shown in (A). The first two peaks on the right are averages of 1.2 ions, the third peak situated at the $z$ coordinate of the inner ring of charges is an average of 1 ion, and the last peak on the intracellular side corresponds to 0.3 ions. These data were calculated over a total simulation period of 1.6 μs.

The blockage of sodium currents by calcium ions demonstrated in our simple model can be understood by studying the energy profiles for various ion configurations. The sodium and calcium single- and multi-ion profiles are plotted together in Fig. 7. We notice that for a negative potential of −94 mV the energy well seen by a single incoming calcium ion is much deeper (~30 kT) than that seen by a sodium ion as shown in Fig. 7A. This is due to the stronger attraction of the divalent ion to the negatively charged residues lining the selectivity filter. This means that calcium ions will be more strongly bound to the selectivity filter region than sodium. This also results in a high energy barrier in the central part of channel which it must surmount if it wants to pass through the channel.

As the selectivity filter is too narrow for ions to pass each other, if a calcium ion enters the selectivity filter, the only way conduction can take place is if it is knocked out of its equilibrium position by other ions. However, in Fig. 7B we show that this is unlikely to occur. If we place one calcium ion in the selectivity filter, and bring another calcium ion into the channel from the right, we see that this second ion is only weakly attracted into the channel by a shallow well in the extracellular vestibule (solid line on right). However, even if a second calcium ion does enter the channel, the first calcium ion sitting in the selectivity filter sees a large energy barrier of 7 kT (lower solid curve) to its left that it must surmount to cross the channel. This barrier is just large enough that we can expect that the calcium ion is unlikely to conduct. Indeed, it is much more likely for the second calcium ion to exit the channel back to the extracellular side than for the first ion to cross the channel.

The resident calcium ion is even less likely to be displaced by an incoming sodium ion. In this case, the sodium ion is again weakly attracted into the channel as indicated by the shallow well in Fig. 7B (dashed line on right). However, for the calcium ion to cross the channel, it

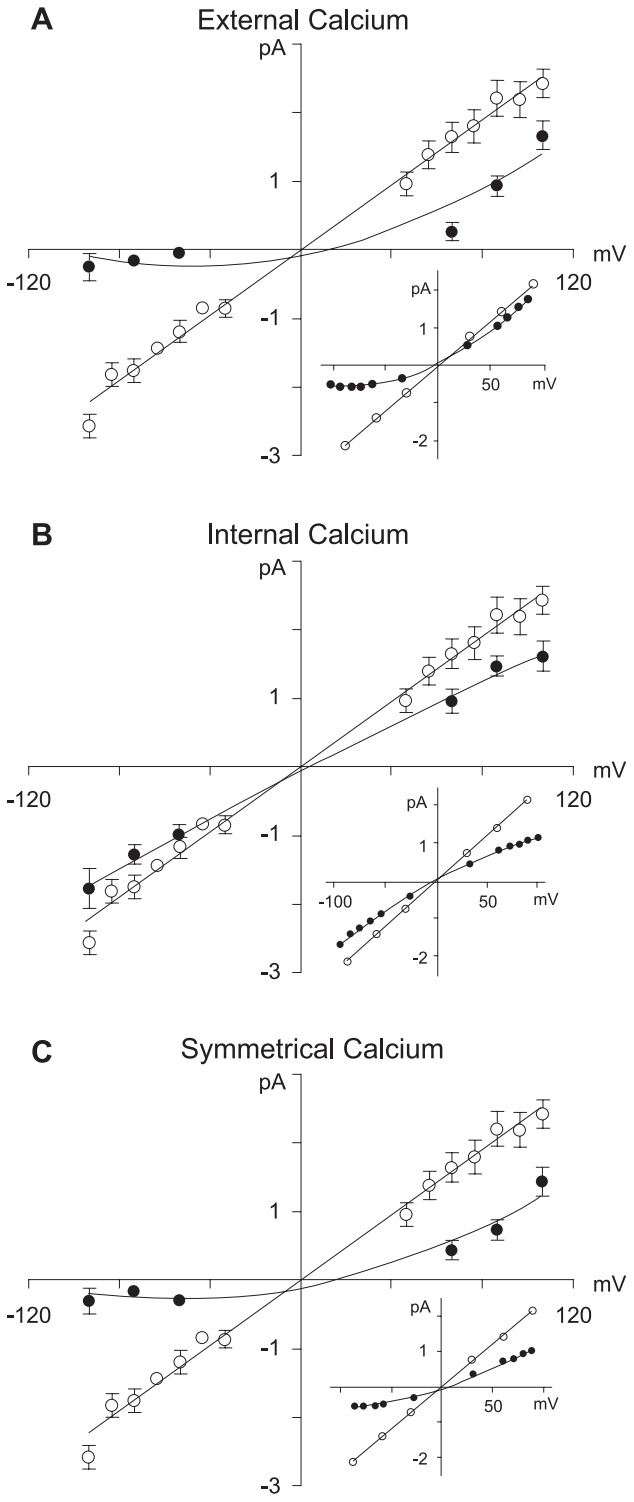


Fig. 6. Current–voltage curves for mixed solutions of NaCl and $CaCl_2$. Open circles represent the current at ±100 mV with pure 200 mM symmetric solutions of NaCl reproduced from Fig. 4A. These data points were collected over 13 μs. Filled circles represent data from the mixed solutions, and each data point represents 6.4 μs. Data by French et al. [16] are depicted in the inset. (A) *I–V* curve obtained with 200 mM NaCl on both sides of the channel, and 110 mM $CaCl_2$ added to external solution. (B) *I–V* curve obtained from symmetrical solutions of 200 mM NaCl and 110 mM $CaCl_2$ added to internal solution. (C) *I–V* curve obtained from symmetrical solutions of NaCl and $CaCl_2$ at 200 and 110 mM, respectively.

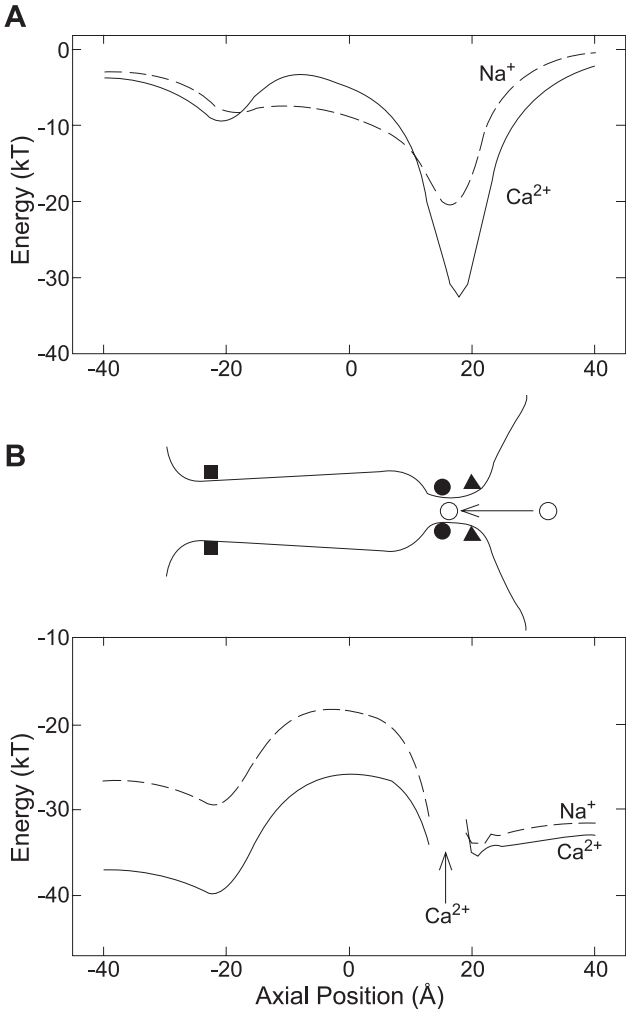


Fig. 7. Single- and multi-ion profiles for mixed solutions. (A) Single-ion profile for a calcium (solid line) and a sodium (dashed line) ion in the channel under an applied potential of −94 mV. (B) Multi-ion energy profiles under an applied potential of −94 mV. A calcium ion is placed in the selectivity filter and the energy of either another calcium (solid line, right hand side) or a sodium ion (dashed line, right hand side) is calculated as it is brought into the channel from the extracellular side. The energy required to move the resident calcium ion to the intracellular side of the channel is then calculated with either a second calcium ion in the filter (solid curve, left hand side) or a sodium ion in the filter (dashed curve, left hand side). An applied potential of −94 mV is used throughout.

faces an energy barrier of 12 kT (upper dashed curve) towards its left, which it finds impossible to overcome. The barrier in this case is much larger than when a second calcium ion enters due to the lower Coulomb repulsion between the ions.

We conclude that once an extracellular calcium ion has entered the selectivity filter, it is very unlikely to cross the channel, even with the assistance of incoming ions of either species. Therefore, this channel cannot be expected to conduct ions, and the presence of a single calcium ion in the channel will block the permeation of sodium ions. This explains the large attenuation of current when calcium is present in the extracellular solution.

On the other hand, an outgoing calcium ion sees a completely different picture, as seen in Fig. 8A. On entering the inner mouth of the channel, it sees an attractive well of only 8 kT followed by an energy barrier of nearly 4.5 kT (solid curve). This attracts the calcium ion only as far as the inner-mouth dipoles, beyond which it faces some resistance. Alternatively, a sodium ion sees an energy well of 23 kT terminating in the selectivity filter (dashed curve). This makes it more likely for a sodium ion to enter the channel before a calcium ion can get in.

When there are two sodium ions present in the selectivity filter (as is usually the equilibrium case, shown in Fig. 5B and later in Fig. 9B), an intracellular calcium ion sees a large insurmountable energy barrier of 11.6 kT in the central part of the channel, seen in Fig. 8B (solid curve on left). This is due to the image forces it experiences in the narrow channel environment. The energy well that draws it into the channel is not deep enough to bind the calcium ion strongly and therefore it hops in and out between this well and the intracellular reservoir. On entering the channel, an intracellular sodium ion sees a barrier of only 3.7 kT (dashed curve on left). This it can overcome with its own thermal energy and cross into the selectivity filter. This explains why a calcium ion is unsuccessful in completely blocking the outgoing current, and yet its occasional presence in the mouth of the channel attenuates the sodium current to a small extent. Therefore, these energy profiles are successful in explaining why extracellular calcium concentrations cause such a large block, whereas intracellular calcium concentrations only partially reduce the current.

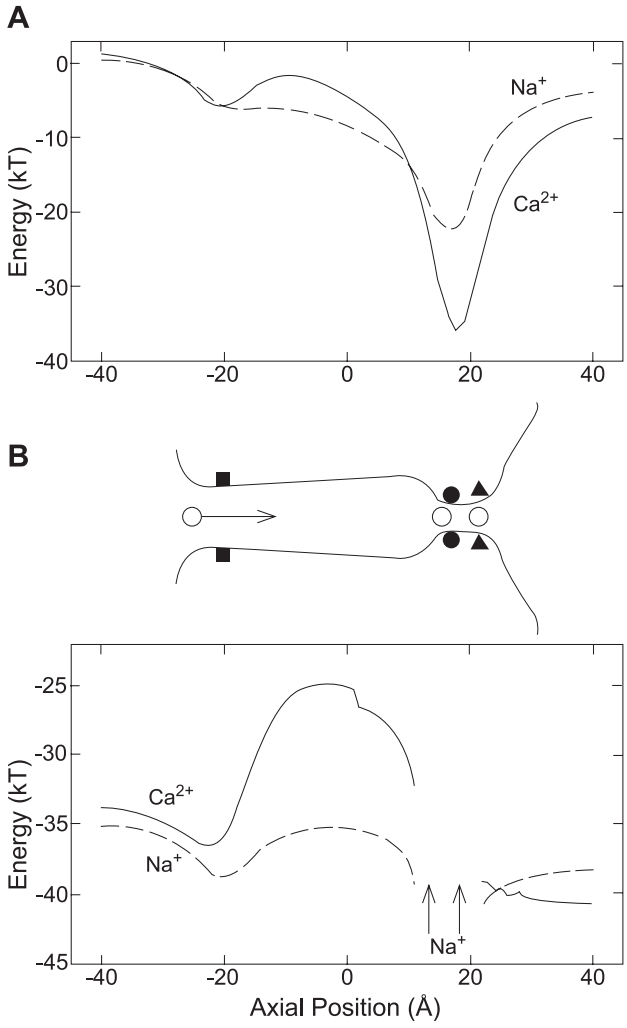


Fig. 8. Single- and multi-ion profiles for mixed solutions. (A) Single-ion profile for a calcium (solid line) and a sodium (dashed line) under an applied potential of +106 mV. (B) A multi-ion profile with two sodium ions held fixed at their equilibrium positions in the selectivity filter, calculated under an applied potential of +106 mV. A sodium ion is brought in from the left and the energy required for it to cross into the selectivity filter is calculated (dashed curve, left hand side). The same is done with an incoming calcium ion (solid curve, left hand side). The energy required to move this sodium ion to the extracellular mouth is calculated first with two sodium ions in the filter (dashed curve, right hand side) and then with calcium and sodium ions in the filter (solid curve, right hand side).

The distribution of ions in the channel with a mixed solution of 200 mM NaCl and 110 mM $CaCl_2$ in the reservoirs obtained from BD simulations under an applied potential of −94 mV is illustrated in Fig. 9A. The large peak in the histogram situated around $z$=18 Å (filled bars) indicates that a calcium ion remains resident in the selectivity filter and remains there for a long time even as other ions wander in and out of the extracellular vestibule. This was expected from the energy profiles above.

The distribution of ions for a positive potential of +106 mV under the same concentrations discussed above is shown in Fig. 9B. It is observed that the second peak of sodium ions at $z$=20 Å (empty bars) is reduced to half its size from that seen in Fig. 5B. This is due to the presence of occasional calcium ions that enter this region from the extracellular side (filled bars). As can be seen from the histogram, no calcium ions are seen inside the channel.

Simulations were also performed with pure 200 mM $CaCl_2$ in the reservoirs. In this case no current was seen to pass through the channel. This supports the conclusion that once a calcium ion has entered the channel, it is virtually stuck there. Only very rarely can it surmount the high central barrier, even with the help of another calcium ion.

## 4. Discussion

We have created a simplified model of voltage-gated sodium channels that can reproduce and explain a large variety of experimental data including the current–voltage and current–concentration relationships for sodium ions, as well as the blockage of sodium currents by calcium ions. The model is based on the structure of the KcsA potassium channel, but with a number of modifications made to comply with various experimental and theoretical studies. If we assume that the broad shape of the channel is similar to that of the KcsA potassium channel, then a relatively unique model arises. We find that only a very small range of shapes

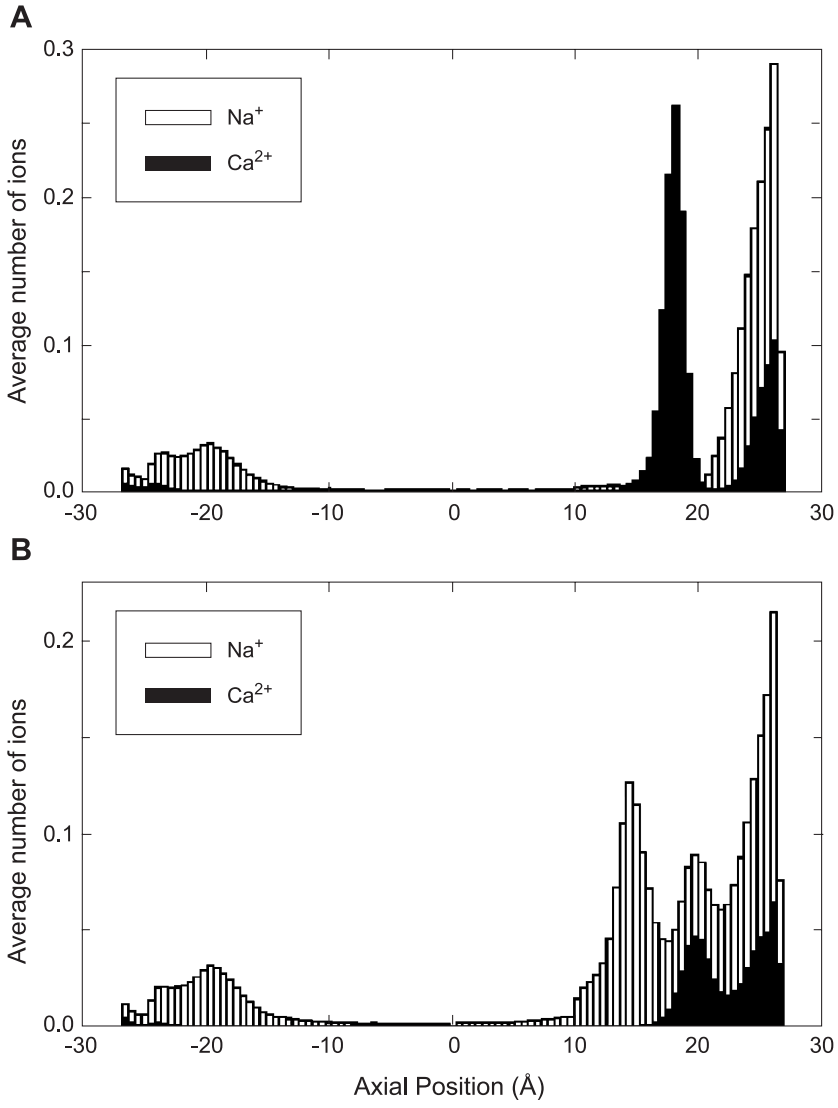


Fig. 9. Histogram showing the average number of calcium (black) and sodium (white) ions in the channel during a simulation at an applied potential of (A) −94 mV and (B) +106 mV. These data were calculated over a total simulation period of 1.6 μs.

and partial charges can reproduce the experimentally determined properties of the channel.

Sodium permeation is seen to involve at least three ions. The selectivity filter is almost always occupied by two sodium ions, and a third ion entering the channel from the extracellular side is required to kick one of the ions across the central region of the channel. Given that measurements have determined a flux ratio exponent of close to 1 [47], and a lower affinity to bind ions than the potassium channel, it may be surprising that we find the channel to always be multiply occupied. However, further reflection shows that this multiple occupancy should not be entirely unexpected. First, sodium ions are clearly less favourably attracted into this channel than potassium ions are into the potassium channel. This can be clearly seen by looking at the single-ion energy profiles. While a single sodium ion is bound by an energy well of around 20 kT in depth in this model (Fig. 3), a potassium ion sees a well of closer to 60 kT in the potassium channel [30,31]. This would explain the different binding affinities.

A number of lines of argument all suggest multiple occupancy of the channel. First, there are a large number of charged residues lining the selectivity filter, six acidic residues and one basic residue. If fully charged, these residues will exert a very strong electrostatic attraction for cations. Indeed, the only way for the channel to not be able to electrostatically bind multiple sodium ions would be either for four of these to be protonated, or for the structure of the channel to be quite different from that of the KcsA channel such that these residues were much farther from the pore. In either case, it would be hard to explain the influence of mutations to any of these residues if they were not imparting a large electrostatic influence to sodium ions [19–21]. Also, we know that calcium ions bind strongly to the channel. If the channel can tightly bind a divalent ion, then it follows that there will also be a large chance that it can

bind two monovalent ions. Indeed, we find the energy wells have to be as deep as shown for this model to correctly reproduce the block of the channel by calcium ions.

All of this, however, seems to conflict with measurements of the flux ratio exponent that find its value to be close to one [47], and are often interpreted as implying that the channel is usually occupied by only one ion. In order to settle this issue, we calculated the flux ratio exponent in our simulations with a concentration and applied potential similar to that used in the experimental study. With external and internal sodium concentrations of 400 and 100 mM, respectively, and an applied potential of +65 mV, we find the flux ratio exponent to be $1.3 \pm 0.3$, only slightly higher than the results found by Begenisich and Busath [47]. Notably, this value is considerably less than the average number of ions in the selectivity filter during the same simulations that was found to be 2.3. These results suggest that some caution needs to be applied when interpreting the meaning of the flux ratio exponent, and one cannot directly equate it to the number of ions in the channel. Indeed, in their original paper, Begenisich and Busath [47] state that their results imply that the sodium channel 'appears to act as a multi-ion pore without a large central barrier'.

The fact that the value of the flux ratio exponent is considerably less than the average number of ions in the channel can be understood if we examine the conditions in which the measurements were made. In the studies of Begenisich and Busath [47], external sodium concentrations of 440 mM were used. An inspection of the current–concentration curve (Fig. 3B), however, indicates that at this concentration, the current passing through the channel is likely to have saturated [2,16,17]. The influx and efflux of ions used to calculate the flux ratio exponent are related to the applied potential and concentration difference across the channel. However, at large concentrations, the fluxes (at least in one direction) will not be concentration-dependent. Therefore, it is possible that the value of the flux ratio exponent calculated at concentrations where the current for the channel has already saturated will be considerably different than at lower concentrations. Clearly, further work is required to better understand the relationship between the flux ratio exponent and the number of coupled ions in the channel.

We also demonstrate how calcium ions attenuate or block sodium currents. Divalent calcium ions are attracted more strongly to the negatively charged residues in the selectivity filter than sodium ions. Thus, at negative potentials it is harder for calcium ions to leave the channel once they have entered from the extracellular side, and this is very rare even with the aid of other calcium or sodium ions in the channel. With extracellular calcium concentrations, and negative potentials, the calcium ions enter and sit in the channel permanently. Alternatively, at positive potentials, these ions still manage to get into the channel and sit alongside a sodium ion (Fig. 9B), but they are not as strongly bound. They temporarily prevent outgoing sodium ions through by presenting a higher central barrier, but once they are replaced by a second sodium ion in the filter, the energy barrier for the outgoing sodium ions is reduced and they are able to cross over the central barrier. This effect only reduces the outward current, but does not completely block it. Thus, the block of the channel by calcium ions is seen to be an electrostatic effect, created by the interaction of the permeating ions with the charged residues in the narrow part of the channel. The narrow width of the filter region is also a key element in the blockage of the channel by divalent ions. This prevents sodium ions from moving past the calcium ion once the latter has entered the channel. We also see that when calcium is present in the intracellular solution it does not permanently block the channel, but hinders the sodium current by briefly occupying the intracellular mouth and preventing sodium ions from getting past.

We have assumed a rigid model, treated water as a continuum and only included a few important partial charges. However, despite these gross simplifications, we are able to gain a valuable insight into some of the characteristic processes of the sodium channel. Furthermore, the fact that the model can reproduce the current–voltage curves in sodium and mixed sodium and calcium solution as well as describing the saturation of current at high concentrations and the blockage of currents by divalent ions gives us confidence in the model. The model we have used in our BD simulations is simple, yet it succeeds in explaining most of the functions of this important class of ion channels.

## Acknowledgements

This work was supported by grants from the Australian Research Council and the National Health and Medical Research Council of Australia. Calculations were done on the Linux Cluster LC and the Alpha server SC of the ANU Supercomputer Facility.

## References

[1] L. Schild, A. Ravindran, E. Moczydlowski, $Zn^{2+}$-induced subconductance events in cardiac $Na^{+}$ channels prolonged by batachotoxin, J. Gen. Physiol. 97 (1991) 117–142.
[2] L. Schild, E. Moczydlowski, Permeation of $Na^{+}$ through open and $Zn^{2+}$-occupied conductance states of cardiac sodium channels modified by batrachotoxin: exploring ion–ion interactions in a multi-ion channel, Biophys. J. 66 (1994) 654–666.
[3] D.L. Kunze, A.E. Lacerda, D.L. Wilson, A.M. Brown, Cardiac Na currents and the inactivating, reopening, and waiting properties of single cardiac Na channels, J. Gen. Physiol. 86 (1985) 691–719.
[4] A.B. Cachelin, J.E. de Peyer, S. Kokubun, H. Reuter, Sodium channels in cultured cardiac cells, J. Physiol. 340 (1983) 389–401.
[5] J.E. Richmond, D.E. Featherstone, H.A. Hartman, P.C. Ruben, Slow inactivation in human cardiac sodium channels, Biophys. J. 74 (1998) 2945–2952.

[6] S.C. Dudley Jr., C.M. Baumgarten, Modification of cardiac sodium channels by carboxyl reagents. Trimethyloxonium and water-soluble carbodiimide, J. Gen. Physiol. 101 (1993) 651–671.
[7] M.E. Gellens, A.L. George Jr., L. Chen, M. Chahine, R. Horn, R.L. Barchi, R.G. Kallen, Primary structure and functional expression of the human cardiac tetrodotoxin-insensitive voltage-dependent sodium channel, Proc. Natl. Acad. Sci. U. S. A. 89 (1992) 554–558.
[8] B. Neumcke, R. Stämpli, Sodium currents and sodium–current fluctuations in rat myelinated nerve fibres, J. Physiol. 329 (1982) 163–184.
[9] F.J. Sigworth, The variance of sodium current fluctuations at the node of Ranvier, J. Physiol. 307 (1979) 97–129.
[10] R.L. Rosenberg, S.A. Tomiko, W.S. Agnew, Single-channel properties of the reconstituted voltage-regulated Na channel isolated from the electroplax of *Electrophorus electricus*, Proc. Natl. Acad. Sci. U. S. A. 81 (1984) 5594–5598.
[11] C.A. Vandenberg, F. Bezanilla, Single-channel, macroscopic and gating currents from Na channels in squid giant axon, Biophys. J. 53 (1988) 226.
[12] C.A. Vandenberg, F. Bezanilla, Single-channel, macroscopic, and gating currents from sodium channels in the squid giant axon, Biophys. J. 60 (1991) 1499–1510.
[13] E.M. Fenwick, A. Marty, E. Neher, Sodium and calcium channels in bovine chromaffin cells, J. Physiol. 331 (1982) 599–635.
[14] W.N. Green, L.B. Weis, O.S. Anderson, Batrachotoxin-modified sodium channels in planar lipid bilayers. Ion permeation and block, J. Gen. Physiol. 89 (1987) 841–872.
[15] R.P. Hartshorne, B.U. Keller, J.A. Talvenheimo, W.A. Catterall, M. Montal, Functional reconstitution of the purified brain sodium channel in planar lipid bilayers, Proc. Natl. Acad. Sci. U. S. A. 82 (1985) 240–244.
[16] R.J. French, J.F. Worley III, W.F. Wonderlin, A.S. Kularatna, B.K. Krueger, Ion permeation, divalent ion block, and chemical modification of single sodium channels, J. Gen. Physiol. 103 (1994) 447–470.
[17] J.F. Worley III, R.J. French, B.A. Pailthorpe, B.K. Krueger, Lipid surface charge does not influence conductance or calcium block of single sodium channels in planar bilayers, Biophys. J. 61 (1992) 1353–1363.
[18] F.J. Sigworth, E. Neher, Single $Na^+$ channel currents observed in cultured rat muscle cells, Nature 287 (1980) 447–449.
[19] S.H. Heinemann, H. Terlau, W. Stühmer, K. Imoto, S. Numa, Calcium channel characteristics conferred on the sodium channel by single mutations, Nature 356 (1992) 441–443.
[20] T. Schlief, R. Schönherr, K. Imoto, S.H. Heinemann, Pore properties of rat brain II sodium channels mutated in the selectivity filter domain, Eur. Biophys. J. 25 (1996) 75–91.
[21] Y.M. Sun, I. Favre, L. Schild, E. Moczydlowski, On the structural basis for size-selective permeation of organic cations through the voltage-gated sodium channel—effect of alanine mutations at the DEKA locus on selectivity, inhibition by $Ca^{2+}$ and $H^+$, and molecular sieving, J. Gen. Physiol. 110 (1997) 693–715.
[22] W.A. Catterall, From ionic currents to molecular mechanisms: the structure and function of voltage-gated sodium channels, Neuron 26 (2000) 13–25.
[23] H.R. Guy, P. Seetharamulu, Molecular model of the action potential sodium channel, Proc. Natl. Acad. Sci. U. S. A. 83 (1986) 508–512.
[24] H.R. Guy, S.R. Durell, Structural Models of $Na^+$, $Ca^{2+}$, and $K^+$ Channels. Ion Channels and Diseases, The Rockefeller University Press, 1995.
[25] G.M. Lipkind, H.A. Fozzard, KcsA crystal structure as framework for a molecular model of the $Na^+$ channel pore, Biochemistry 39 (2000) 8161–8170.
[26] C. Sato, Y. Ueno, K. Asai, K. Takahashi, M. Sato, A. Engel, Y. Fujiyoshi, The voltage-sensitive sodium channel is a bell-shaped molecule with several cavities, Nature 409 (2001) 1047–1051.
[27] D.A. Doyle, J.M. Cabral, R.A. Pfuetzner, A. Kuo, J.M. Gulbis, S.L. Cohen, B.T. Chait, R. MacKinnon, The structure of the potassium channel: molecular basis of $K^+$ conduction and selectivity, Science 280 (1998) 69–77.
[28] B. Hille, The permeability of the sodium channel to organic cations, J. Gen. Physiol. 58 (1971) 599–619.
[29] B. Corry, T.W. Allen, S. Kuyucak, S.H. Chung, Mechanisms of permeation and selectivity in calcium channels, Biophys. J. 80 (2001) 195–214.
[30] S.H. Chung, T.W. Allen, S. Kuyucak, Modeling diverse range of potassium channels with Brownian dynamics, Biophys. J. 83 (2002) 263–277.
[31] S.H. Chung, T.W. Allen, M. Hoyles, S. Kuyucak, Permeation of ions across the potassium channel: Brownian dynamics studies, Biophys. J. 77 (1999) 2517–2533.
[32] D.G. Levitt, Electrostatic calculations for an ion channel: I. Energy and potential profiles and interactions between ions, Biophys. J. 22 (1978) 209–219.
[33] M. Hoyles, S. Kuyucak, S.H. Chung, Energy barrier presented to ions by the vestibule of the biological membrane channel, Biophys. J. 70 (1996) 1628–1642.
[34] T.W. Allen, S. Kuyucak, S.H. Chung, Molecular dynamics estimates of ion diffusion in model hydrophobic and KcsA potassium channels, Biophys. Chem. 86 (2000) 1–14.
[35] W.F. van Gunsteren, H.J.C. Berendsen, J.A. Rullmann, Stochastic dynamics for molecules with constraints: Brownian dynamics of *n*-alkanes, Mol. Phys. 44 (1981) 69–95.
[36] W.F. van Gunsteren, H.J.C. Berendsen, Algorithms for Brownian dynamics, Mol. Phys. 45 (1982) 637–647.
[37] S.H. Chung, T.W. Allen, M. Hoyles, S. Kuyucak, Study of ionic currents across a model membrane channel using Brownian dynamics, Biophys. J. 75 (1998) 793–809.
[38] A. Ravindran, L. Schild, E. Moczydlowski, Divalent cation selectivity for external block of voltage dependant $Na^+$ channels prolonged by batrochotoxin. $Zn^{2+}$ induces discrete substates in cardiac $Na^+$ channel, J. Gen. Physiol. 97 (1991) 89–115.
[39] R.E. Taylor, C.M. Armstrong, F. Bezanilla, Block of sodium channels by external calcium ions, Biophys. J. 16 (1976) 27.
[40] J. Tanguy, J.Z. Yeh, Divalent cation block of normal and BTX-modified sodium channels in squid axons, Biophys. J. 53 (1988) 229.
[41] D. Yamamoto, J.Z. Yeh, T. Narahashi, Voltage-dependent calcium block of normal and tetramethrin-modified single sodium channels, Biophys. J. 45 (1984) 337–344.
[42] A.M. Woodhull, Ionic blockage of sodium channels in nerve, J. Gen. Physiol. 61 (1973) 687–708.
[43] G.N. Mozhayeva, A.P. Naumov, B.I. Khadorov, Potential dependent blockage of batrachotoxin-modified sodium channels in frog node of Ranvier by calcium ions, Gen. Physiol. Biophys. 1 (1982) 281–282.
[44] J.F. Worley III, R.J. French, B.K. Krueger, Trimethyloxonium modification of single batrachotoxin-activated sodium channels in planar bilayers, J. Gen. Physiol. 87 (1986) 327–347.
[45] R.J. French, J.F. Worley III, W.F. Wonderlin, A.S. Kularatna, B.K. Krueger, Description by single- and double-occupancy rate-theory models, J. Gen. Physiol. 103 (1994) 447–470.
[46] E. Moczydlowski, A. Uehara, X. Guo, J. Heiny, Iso-channels and blocking modes of voltage-dependent sodium channels, Ann. N. Y. Acad. Sci. 479 (1986) 269–292.
[47] T. Begenisich, D. Busath, Sodium flux ratio in voltage-clamped squid giant axons, J. Gen. Physiol. 77 (1981) 489–502.